JOURNAL OF AIRCRAFT
Vol. 38, No. 3, May–June 2001

Theoretical and Experimental Investigation of Biplane Delta Wings

Lance W. Traub*
Texas A&M University, College Station, Texas, 77843-3141

Recent interest in micro aerial vehicles has resulted in the evaluation of innovative aerodynamic configurations and propulsive mechanisms to meet the requirements of these machines. It is proposed that a biplane formed using delta wings may prove to be an efficient configuration. Accordingly, a theoretical and experimental investigation to determine the characteristics of delta wings in a biplane configuration was undertaken. The wind-tunnel study was performed using 75-deg delta wings. The biplane wing's gap (separation) and stagger were varied. A theoretical method was developed that coupled Prandtl's biplane theory (Prandtl, L., and Tietjens, O. G., *Applied Hydro and Aeromechanics*, Dover, New York, 1934, pp. 211–222) with Polhamus' leading-edge suction analogy (Polhamus, E. C., "Prediction of Vortex-Lift Characteristics by a Leading-Edge Suction Analogy," *Journal of Aircraft*, Vol. 8, No. 4, 1971, pp. 193–199). The experimental results showed that the separation between the wings has a significant effect on lift, the lift reducing with closer wing proximity. The biplane configuration shows far less sensitivity to stagger, with effects only manifesting for angles of attack greater than 15 deg. Positive stagger (upper wing forward) increased lift whereas negative stagger decreased lift relative to an unstaggered configuration. Similarly, positive stagger increased the maximum recorded lift coefficient with negative stagger having the opposite effect. The theoretical method showed close accord with the experimental data and correctly predicted the effect of gap and stagger on lift. Theoretical analysis showed that for a dimensionally constrained planform, the delta wing biplane is an effective configuration for moderate to large wing separation.

Nomenclature

a	=	geometric parameter, m
b	=	wing span, m
C_D	=	drag coefficient
C_L	=	lift coefficient
$C_{L\alpha}$	=	lift curve slope
C_r	=	wing root chord, m
h	=	geometric parameter, m
K_P	=	potential constant
K_V	=	wing vortex lift constant
L	=	lift, N
q	=	dynamic pressure, Pa
r	=	geometric parameter, m
S	=	wing area, m^2
U	=	freestream velocity, m/s
U_{12}	=	induced axial velocity increment, m/s
V	=	induced velocity, m/s
W	=	normal component of induced velocity, m/s
X	=	stagger, m
x, y, z	=	Cartesian coordinates, m
y_1	=	point of interest
Z	=	gap, m
Z'	=	effective or average gap, m
α	=	geometric angle of attack, deg
α_{12}	=	angle of attack induced on wing 1 by wing 2, deg
β	=	geometric parameter, deg
Γ	=	bound circulation, m^2/s
Γ_0	=	wing root circulation, m^2/s
γ	=	geometric parameter, deg
δ	=	efficiency factor
ϵ	=	wing apex angle, deg
Λ	=	wing leading-edge sweep angle, deg
λ	=	geometric parameter, deg
ϕ	=	geometric parameter, deg

Subscripts

at	=	attached
B	=	bound
bip	=	biplane
i	=	induced
l	=	lower
min	=	minimum
mono	=	monoplane
T	=	trailing
tot	=	total
u	=	upper
1	=	wing 1
2	=	wing 2
2D	=	two dimensional
3D	=	three dimensional
12	=	effect on wing 1 of wing 2

Superscript

$\cdot$	=	incorporates axial velocity increment

Received 29 February 2000; revision received 1 September 2000; accepted for publication 18 September 2000.

*Postdoctoral Research Associate, Aerospace Engineering Department. Associate Member AIAA.

Introduction

EARLY flight endeavors led to the prominence of the multiplane configuration. The moderate lifting performance and structural integrity of early flying machines found redemption in the biplane configuration. Subsequent structural and aerodynamic advances found the biplane falling into disfavor in the early 1930s. For a constrained wing span, however, biplanes do possess aerodynamic efficiency advantages as compared to monoplanes. At a given lift coefficient and assuming elliptic loading, the vortex drag of a biplane tends to half that of a monoplane as the separation distance between the wings tends to infinity [vortex drag of the monoplane is given by $C_L^2/\pi AR$ and that of the biplane by $(C_L/2)^2/\pi AR + (C_L/2)^2/\pi AR = C_L^2/2\pi AR$]. The biplane distributes the trailing vorticity over an appreciable area, thus, reducing the downwash at a point and, consequently, reducing vortex drag. Alternatively, the biplane captures a larger volume of air that is accelerated down to

generate the lift impulse, thus reducing the downwash velocity and, hence, the kinetic energy imbued to the accelerated fluid.

Experimental studies[1–4] were conducted in the 1920s to determine characteristics of biplanes, that is, the effects of stagger, wing separation (gap), decalage (angle between the chord lines of the wings), dihedral, relative wing spans, and sweep. Using reflection plane models, Knight and Noyes[1] used surface pressure integration to determine the effects of decalage, dihedral, sweepback, and wing overhang (differing spans). The tests were uncorrected for wall effects and were conducted at $Re = 1.5 \times 10^5$; they are subject to scale effects. Nonetheless, the trends should still be valid. In all instances, the recorded normal force coefficient based on the total wing area was lower than that of a monoplane consisting of an individual biplane wing. For no stagger, variations of the decalage angle of 3 and 6 deg (by varying the lower wing's incidence) showed that positive decalage (lower wing at a higher geometric α than the upper wing) increased the cellule normal force coefficient; negative decalage had the opposite effect. Positive decalage reduced the normal force coefficient on the upper wing, but greatly increased it on the lower wing. The opposite effect was noted for negative decalage. The dihedral angle explored (3 deg) was found to have a weak effect on the total normal force coefficient recorded. The effects of two wing leading-edge sweep angles were investigated (5 and 10 deg). Sweepback was found to have a negligible effect on the cellule normal force coefficient, although the load distributions between the wings was moderately affected. The effect of differing wing overhangs (spans) was also investigated for $b_u/b_l = 1.25$, $b_l/b_u = 0.8$, and $b_l/b_u = 0.6$. The net effect on the normal force coefficient was small. The distribution of the wing loads was affected, with the individual wing's AR generally dictating its loading, for example, that with higher AR showed higher loading. A similar study by the same researchers[2] at the same test conditions showed that positive stagger (upper wing forward) increases the cellule normal force coefficient moderately, whereas negative stagger has the opposite effect. A similar result was found by Norton.[3] The loading on the upper wing was increased by positive stagger (and decreased by negative stagger), whereas that on the lower wing was far less receptive to stagger changes (negative stagger was found to increase lower wing loading slightly). Increasing the wing gap ($Z/C_r = 0.5 \rightarrow 1.5$) showed a marked increase in the total normal force coefficient. Regarding the individual wing loading, the effect of the wing gap was profound on the upper wing and slight on the lower wing.

Subsequently, Prandtl[5] extended his lifting line theory to biplanes, allowing theoretical estimation of the effect of the primary design variables, stagger and gap, as well as the relative size of the wings. The theory[5] revealed interesting interference characteristics: For an unstaggered biplane the drag increments due to the mutual influence of the wings are equal and are always additive. For a staggered biplane, both the bound and trailing vortices of each wing influence the other. Thus, for positive stagger (the upper wing in front of the lower wing) the upper wing increases the downwash on the lower wing, thus increasing its drag, and vice versa for the effect of the lower wing on the upper wing. Munk[6] showed that the total mutual induced drag of a biplane for a fixed gap is independent of the amount of stagger (Munk's stagger wing theorem). This theorem is only valid if the two wings' lift distributions are unaltered (through varying the wings' α). For multiplanes, minimum drag of the system is achieved when the induced downwash velocities on the wings are equal and constant along the span, as is the case for a monoplane. Drag is also minimized by matching the span of the biplane's wings.

Recent interest in small-scale unpiloted aerial vehicles has promulgated investigation of numerous nonconventional wing and propulsion configurations.[7] The inherent utility of micro aerial vehicles has promulgated an intense research effort to supply the necessary technology. Generally, research efforts have followed two distinct paths. Microvehicles have been designed that use relatively conventional planforms: canard-trapezoidal wings, circular wings, or, perhaps, less conventional ring wings. Unfortunately, these wings are inherently limited by design to be relatively inefficient at the extremely low Reynolds numbers ($<5 \times 10^4$) at which a microvehicle may operate. In the Reynolds number range of interest, the flow is laminar, limiting the lift that may be generated and causing the wings to be prone to laminar separation effects with concomitant large losses of lift, high drag, and potential loss of control power. Compounding the problem is the nature of the environment in which these wings operate, close to the surface such that the atmosphere is intrinsically gusty. This places even greater requirements on the wing form in that it should be relatively insensitive to atmospheric turbulence. The second research area has been to design vehicles that utilize propulsive-lift mechanisms evolved in nature, that is, biologically inspired.[8] Incorporation of biological kinematics into microvehicle design presents formidable challenges. First, the wing kinematics and structures used by insects are not completely understood. Consequently, any attempt at emulating insect flight mechanisms will be, at best, an approximation. Second, the wing kinematics used by insects present significant problems to simulate.

The Reynolds number behavior of delta wings is relatively unique. Virtually every facet of delta wing flow physics is largely independent of the Reynolds number. Through enforced leading-edge separation, the flow over a delta is dominated by the formation of large leading-edge vortices that greatly enhance lift and allow delta wings to operate at high angles of attack. This lift augmentation is necessary because delta wings, due to their low AR, are inherently poor lift generators. Experimental studies[9] have verified that sharp-edged delta wings are insensitive to Reynolds numbers, and have similar lifting characteristics at a $Re = 2 \times 10^4$ or 1.14×10^6. Additionally, due to their low lift-curve slopes, delta wings are not particularly sensitive to atmospheric gusts or disturbances.

Within the limited dimensional confines of a micro aerial vehicle, the lifting performance of a delta wing is unlikely to be satisfactory, perhaps requiring high cruise speeds. A means to circumvent this problem would be to use nonplanar wings, that is, a biplane configuration. The dual wings may allow sufficient lift generation (lift coefficients greater than 2.5 compared to a monoplane wing with equivalent projected area) for all envisaged operations. It would not be necessary to employ any unsteady lift generating mechanisms to augment lift, greatly simplifying the vehicle. The configuration would still benefit from all of the favorable characteristics of delta wings, that is, stable lift generation to high angles of attack, insensitivity to Reynolds number effects, and attenuated response to gusts. For a micro aerial vehicle with a constrained span, biplanes are a highly efficient configuration and, when combined with the features of delta wings, may comprise an excellent configuration to meet the requirements for this type of vehicle.

The lifting characteristics of slender planar sharp-edged delta wings can be accurately estimated using Polhamus'[10] leading-edge suction analogy. Polhamus surmised that, for a sharp-edged delta wing, the lost leading-edge suction was recovered as vortex lift if the flow reattached inboard of the vortices on the upper wing surface, i.e. the leading-edge suction vector was effectively rotated through 90 deg to the plane of the normal force. The total lift on a delta wing is then constituted of a potential component quantified as the attached flow lift in the absence of leading-edge suction and a vortex lift component. A major strength of the suction analogy is its utility and accuracy.

Consequently, to verify the practicality of the biplane delta configuration and to extend the database on delta wing configurations, a low-speed wind-tunnel investigation and theoretical analysis have been undertaken. The theoretical analysis merges Polhamus' suction analogy[10] and Prandtl's biplane theory[5] to allow estimation of the interference effects on lift. Prandtl's biplane theory does not account for the effect of the mutual wing interference on lift; in the present analysis, the theory is extended to account for this interaction. This type of theoretical approach allows explicit identification of the relationship between design variables and aerodynamic characteristics. Comparisons between the present experimental data and the theoretical prediction method are presented.

Model Description and Experimental Procedure

Figure 1a shows geometric details of the models used in the study. All of the wings were fabricated from mild steel plate. Wentz and

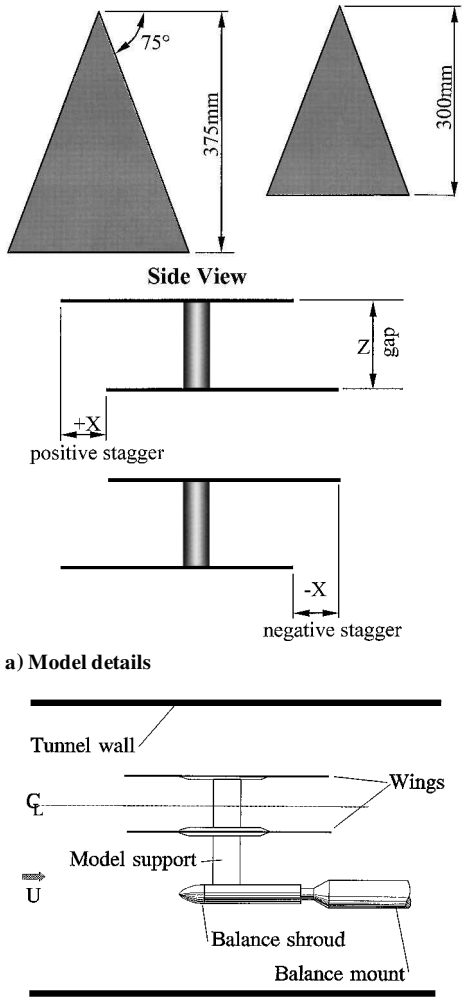

Fig. 1 Geometrical details of wind-tunnel mount and models.

Kohlman[11] found for a series of wings (thickness/$C_r = 1.1\%$) that a square-edged wing showed similar performance characteristics to a chamfered or bevelled-edged wing. Consequently, to eliminate the necessity of bevelling the wing's leading edges, the wings were manufactured from 1.52-mm-thick steel plate. The wing's thickness, combined with a root chord of 300 mm, yields a thickness to chord ratio of 0.51%. A leading-edge sweep angle of 75 deg was investigated. Larger wings of 375-mm root chord were also manufactured to investigate potential blockage effects and disparate wing sizes.

In the tests, both wing separation (gap) and axial spacing (stagger) were investigated. For zero stagger, wing gaps of $Z/C_r = 0.25$, 0.33, and 0.42 were evaluated. For a wing gap of $Z/C_r = 0.42$, the upper and lower wings were staggered at $X/C_r = \pm 0.17$ and 0.33 with positive stagger indicating a forward upper wing. The wings were attached to a mount that consisted of a thin reinforcing spine that extended for 203 mm along the root chord of the wing, to minimize wing flexing (see Fig. 1b). At no time during the testing was any chordwise or spanwise flexing of the models observed. The model dimensions were kept to a minimum to reduce the effect of the wind-tunnel walls. Tests were undertaken in Texas A&M University's 3×4 ft continuous wind tunnel at $U = 38$ m/s and $Re = 0.77 \times 10^6$ based on C_r. All of the presented experimental data for the biplane configurations were reduced by the total wing area, unless mentioned otherwise. A six-component Aerolab sting balance was used for force determination. The accuracy of this balance is estimated at 0.5% of the maximum measured lift and drag. Balance resolution is better than 2×10^{-4} of the measured coefficient on all channels. Through repeated data runs, repeatability of the balance for lift and drag is estimated at $\Delta C_L = 0.0008$ and $\Delta C_D = 0.0005$. Model pitch and yaw is adjusted using dc motors connected through a potentiometer to a digital readout display. Model angle of attack can be set to within 0.05 deg. Force balance data as well as tunnel dynamic pressure were acquired using a personal computer equipped with a 16-bit A/D board. The data acquisition program used to acquire the balance loads samples each data channel 1000 times and averages it.

The force balance tests comprised pitching the model through a set angle of attack range from -2 to 56 deg. Data were recorded at 2-deg intervals. Delta wing flows, assuming enforced leading-edge flow separation, are not particularly sensitive to Reynolds number or scale effects, although the location of the secondary separation is Reynolds number dependent. In an effort to be consistent with other investigations,[12,13] it was decided not to employ any type of forced transition as enforced transition does not guarantee a flowfield representative of realistic flight Reynolds numbers. Tare and interference effects were determined using an image system[14] as this method is relatively simple to implement and yields the total interference and tare effects and additionally may be used to determine the wind-tunnel flow angularity. In this study, solid and wake blockage were corrected for using the method of Shindo.[15] Upwash corrections were applied using the method detailed by Rae and Pope.[14]

Experimental Results

As all of the models used in the investigation were thin (and essentially sharp edged), uncambered, and planar, their drag behavior is uniquely defined by lift; $C_D = C_{D\,\min} + C_L \tan\alpha$. Consequently, it is not necessary to present drag results to characterize relative wing performance. Although the level of blockage in the majority of the tests was generally low ($\approx 3.8\%$ at $\alpha = 60$ deg), it was deemed necessary to evaluate if significant blockage effects were present. Figure 2 shows a comparison between the $C_r = 0.3$ and 0.375 m wings. Blockage for the larger wings is 53% greater, that is, 5.8%. The data show that blockage/wall effects were generally small and negligible for $\alpha < 25$ deg.

Figure 3 presents the effect of gap on lift coefficient for zero stagger. Also included are data for a monoplane delta. It is apparent that wing separation has a significant impact on both the potential and vortex lift. Reduction in the potential or attached flow lift is evident by the marked reduction in lift at low α (less than 10 deg), and the attenuation of vortex lift is visible in the reduced nonlinearity of the curves. The mutual induced interference of the wings results in increased downwash that both attenuates the attached flow lift by reducing the wing's effective angle of attack and reduces the vortex lift by increasing the vortex drag, which, consequently, reduces the leading-edge thrust. These effects will be clarified later in the theoretical development. Compared to the monoplane, the biplane configurations possess a noticeably more docile stall. For a 75-deg sweep delta, the onset of vortex breakdown at the wing trailing edge is associated with abrupt wing stall. It is likely that the channel that the leading-edge vortices of the lower wing are confined to affects the burst characteristics of these vortices as they now are affected by the pressure fields of both the upper and lower wings. Thus,

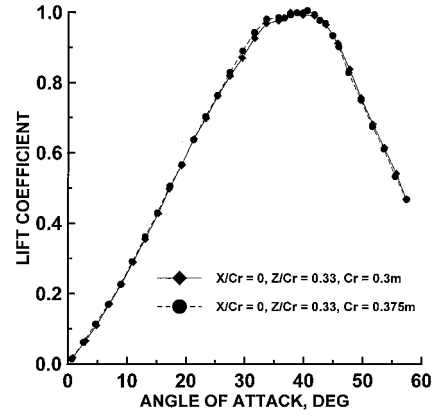

Fig. 2 Effect of dissimilar model size on the measured lift coefficient.

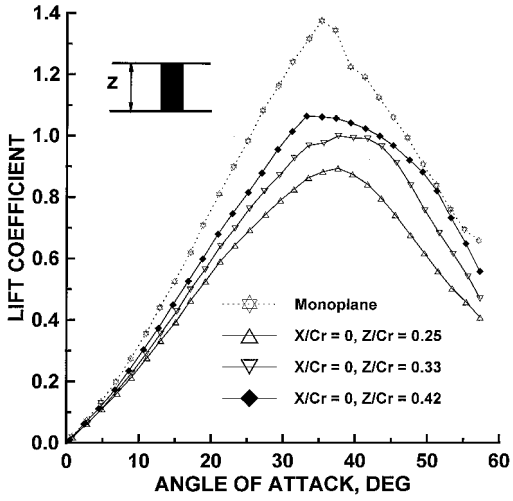

Fig. 3 Effect of wing gap on the measured lift coefficient.

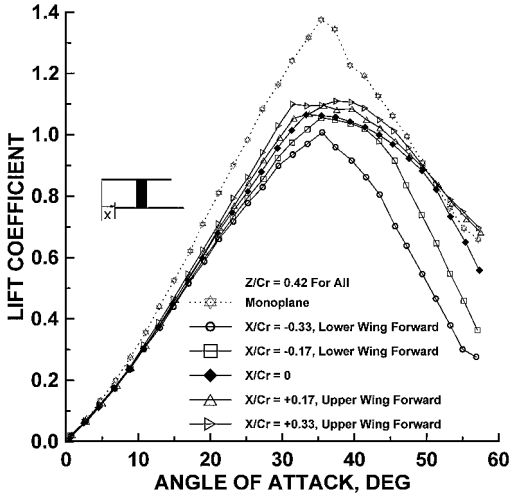

Fig. 4 Effect of wing stagger on the measured lift coefficient.

bursting of the upper and lower vortices at dissimilar incidence would lead to a moderation of the severity of stall. Compared to the monoplane wing, the biplanes show a steadily increasing lift decrement with decreasing Z/C_r. Note that the physical lift (in Newtons) that would by developed by the biplane wing is twice that indicated in Fig. 3 (the biplane wings have twice the area of the monoplane wing). For a confined planform lifting vehicle, the biplanes would generate significant lift, although not as effectively as two infinitely separated wings.

The effect of wing stagger for a fixed gap of $Z/C_r = 0.42$ is shown in Fig. 4. At low α, the effects of the range of stagger explored on the lift coefficients are marginal, which, as will be shown later, does not imply that the individual loading on the wings is unaffected, but that the total loading is invariant. At higher incidence ($\alpha > 20$ deg) the impact of stagger becomes marked. Positive stagger (upper wing forward) increases lift, whereas negative stagger has the opposite effect. A weaker but similar trend is seen in the data of Knight and Noyes.[2] For the delta biplanes, the data suggest that stagger has the most significant impact on the vortex lift. Geometrical consideration indicates that the trajectories and imposed adverse pressure gradient experienced by the leading-edge vortices of the lower wing are affected most by the biplane configuration. Consequently, positive stagger may reduce the extent of the channel that the lower wing's vortices must negotiate. Additionally, the positive pressures associated with the windward surface of the upper wing increase the adverse pressure gradient the vortices must negotiate as they pass near the trailing edge of the wing, where the vortices trajectories bring them into closer proximity with the upper wing. Vortex breakdown is sensitive to the vortices' swirl ratio (ratio of the maximum rotary velocity at the edge of the viscous core to the maximum, or average, core axial velocity) and imposed adverse pressure gradient. It is unlikely that the wing interference would increase the lower vortices' swirl ratio (this would generally encompass strengthening the vortex). Thus, earlier breakdown of the lower wing vortices may be precipitated by an increased adverse pressure gradient. Positive stagger may, thus, beneficially alter the lower surface vortices trajectory to mitigate/lessen the adverse impact of the upper wing's windward compression surface. Poststall lift generation is greatly reduced by negative stagger. Although not verified experimentally, the lift loss is most likely associated with an accelerated forward progression of vortex breakdown of the lower wing's vortices.

Theoretical Prediction Method

Analysis of delta wings using slender wing theory consists of evaluation of the flow in a crossflow plane at any chordwise location. The flow patterns at a chordwise location are similar, and the wing extends to infinity downstream. Consequently, each chordwise plane of the wing is essentially a Trefftz plane. The solution for the crossflow plane is then integrated chordwise to yield the properties of the wing (trailing-edge influences excluded). In lifting line theory, the wing is replaced by a bound vortex located at the wing's quarter chord. The no-penetration condition is enforced at the three-quarter chord location of the wing. The bound vortex sheds a continuous sheet of trailing vorticity to avoid violating Helmholtz's theorems. This sheet is assumed to remain flat and extend downstream to infinity. The solution of the flow can be determined from the crossflow at infinity downstream (Trefftz plane). The downwash induced by the trailing vortex system at the wing is then half that at the Trefftz plane.

In the present analysis, perhaps somewhat unconventionally, the wings are replaced by two lifting lines with each embodying the three-dimensional wing's properties. Although the specific chordwise locations of the lifting lines are not required, the relative chordwise location of the two lifting lines is germane. They are effectively placed at the wing's trailing edge to ensure that the spanwise integration variables are correct, that is, $\pm b_{1,2}/2$. The methodology accounts for effects of gap, stagger, dissimilar wing size, and sweep. A schematic of the lifting line layout and describing variables is shown in Fig. 5.

In order to allow realization of simple explicit relations, it is necessary to outline some simplifying assumptions implemented in the analysis:

1) Both wings of the biplane cellule have elliptic loading. Jones'[16] slender wing theory shows that the attached flow spanwise load distribution on a slender delta wing is elliptic.

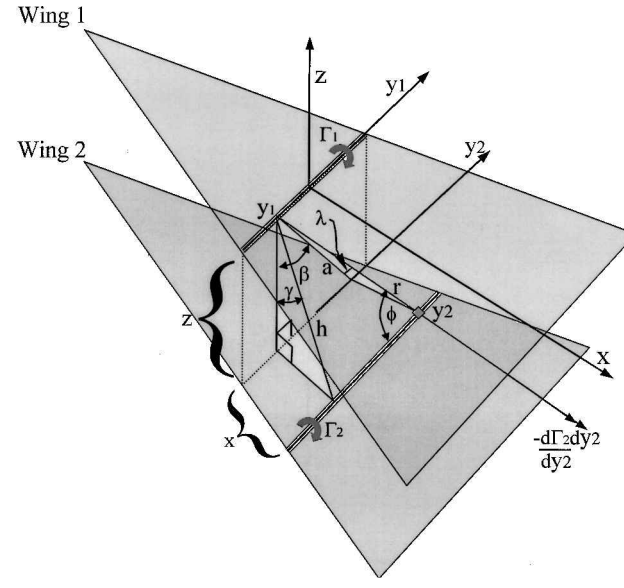

Fig. 5 Staggered biplane descriptive variables.

2) The unperturbed elliptic load distribution (of each wing acting as a monoplane) is used to determine the velocity induced on the other wing and the wing's own loading.

3) Effects of decalage are not accounted for.

At point y_1 on wing 1, the vortex system of wing 2 induces a velocity due to its bound and trailing vortex system. The bound vortex system of wing 2 also induces an axial velocity component at the lifting line of wing 1. Although this component is generally considered to be small,[5] it is included in the analysis.

The velocity induced at wing 1 (point y_1) due to a strip of the trailing vortex of wing 2 can be determined using the Biot–Savart law[5]:

$$\mathrm{d}V_{12T} = \int_{\lambda}^{\pi/2} \frac{1}{4\pi a}\left(-\frac{\mathrm{d}\Gamma_2}{\mathrm{d}y_2}\,\mathrm{d}y_2\right)\cos\lambda$$

$$= \frac{-1}{4\pi a}\left(\frac{\mathrm{d}\Gamma_2}{\mathrm{d}y2}\,\mathrm{d}y2\right)(1-\sin\lambda) \tag{1}$$

The vertical component of this velocity is

$$\mathrm{d}W_{12T} = \frac{-1}{4\pi a}\left(\frac{\mathrm{d}\Gamma_2}{\mathrm{d}y_2}\,\mathrm{d}y_2\right)(1-\sin\lambda)\sin\beta \tag{2}$$

The total normal velocity at y_1 due to the trailing vortex sheet of wing 2 is

$$W_{12T} = \frac{-1}{4\pi}\int_{-b_2/2}^{b_2/2}\frac{1}{a}\frac{\mathrm{d}\Gamma_2}{\mathrm{d}y_2}(1-\sin\lambda)\sin\beta\,\mathrm{d}y2 \tag{3}$$

To facilitate the analysis, use is made of the following relationships (see Fig. 5):

$$\sin\lambda = X/r \tag{4a}$$

$$\sin\beta = (y2 - y_1)/a \tag{4b}$$

$$r = \sqrt{a^2 + X^2} \tag{4c}$$

$$a = \sqrt{(y2-y_1)^2 + Z^2} \tag{4d}$$

$$\sin\phi = h/r \tag{4e}$$

$$\sin\gamma = X/h \tag{4f}$$

$$\cos\gamma = Z/h \tag{4g}$$

yielding

$$W_{12T} = \frac{-1}{4\pi}\int_{-b_2/2}^{b_2/2}\frac{1}{a^2}\frac{\mathrm{d}\Gamma_2}{\mathrm{d}y_2}\left(1-\frac{X}{r}\right)(y2-y_1)\,\mathrm{d}y2 \tag{5}$$

This expression, for an assumed elliptic spanwise load distribution, is singular at the wing tips ($\pm b/2$). This can be circumvented using integration by parts.[5] Noting that the circulation tends to zero at the wing tips yields

$$W_{12T} = \frac{-1}{4\pi}\int_{-b_2/2}^{b_2/2}\Gamma_2(y2)$$

$$\times\left[\frac{a^2-2(y2-y_1)^2}{a^4}\left(1-\frac{X}{r}\right) - \frac{X(y2-y_1)^2}{a^2r^3}\right]\mathrm{d}y2 \tag{6}$$

The velocity at y_1 due to a bound vortex element of wing 2 is

$$\mathrm{d}V_{12B} = \frac{\Gamma_2\sin\phi\,\mathrm{d}y_2}{4\pi r^2} = \frac{\Gamma_2(h/r)\,\mathrm{d}y_2}{4\pi r^2} \tag{7}$$

Thus, the normal velocity component induced at y_1 due to an element of the bound vortex of wing 2 is

$$\mathrm{d}W_{12B} = \frac{\Gamma_2 h\,\mathrm{d}y_2\sin\gamma}{4\pi r^3} \tag{8}$$

The total induced normal velocity at y_1 due to the wing 2 bound vortex is

$$W_{12B} = \int_{-b_2/2}^{b_2/2}\frac{\Gamma_2 X}{4\pi r^3}\,\mathrm{d}y2 \tag{9}$$

The total vertical or normal velocity induced by wing 2 at location y_1 of wing 1 is

$$W_{12\mathrm{tot}} = W_{12T} + W_{12B} \tag{10}$$

The axial velocity component induced at y_1 due to an element of the bound vortex of wing 2 is

$$\mathrm{d}U_{12B} = \frac{-\Gamma_2 h\,\mathrm{d}y_2\cos\gamma}{4\pi r^3} \tag{11}$$

where the negative sign is required due to the sign convention. The total induced axial velocity at point y_1 is then

$$U_{12B} = \int_{-b_2/2}^{b_2/2}\frac{-\Gamma_2 Z}{4\pi r^3}\,\mathrm{d}y2 \tag{12}$$

The total axial velocity is

$$U_{\mathrm{tot}} = U + U_{12B} = U(1 + U_{12B}/U) \tag{13}$$

For wing 1 or 2, the assumed spanwise load distribution is given by

$$\Gamma = \Gamma_0\sqrt{1-(2y/b)^2} \tag{14}$$

For elliptic loading, we may write the Kutta–Joukowski theorem as (noting that the effective vortex span of the wing is $\pi/4$)

$$L = \rho U\Gamma_0 b(\pi/4) = C_{L\alpha\,3\mathrm{D}}\sin\alpha\tfrac{1}{2}\rho U^2 S \tag{15}$$

which gives

$$\Gamma_0 = (2/\pi)U(S/b)C_{L\alpha\,3\mathrm{D}}\sin\alpha \tag{16}$$

which, with $S/b = C_r/2$ for a delta wing, yields

$$\Gamma_0 = (C_r/\pi)UC_{L\alpha\,3\mathrm{D}}\sin\alpha \tag{17}$$

Thus, the change in the local α of wing 1 at point y_1 due to wing 2 may be expressed as

$$\alpha_{12}(y_1) = \frac{W_{12\mathrm{tot}}}{U} = \frac{-1}{4\pi^2}\int_{-b_2/2}^{b_2/2}C_{r2}C_{L\alpha\,3\mathrm{D}_2}\sin\alpha\sqrt{1-\left(\frac{2y_2}{b_2}\right)^2}$$

$$\times\left[\frac{a^2-2(y2-y_1)^2}{a_4}\left(1-\frac{X}{r}\right) - \frac{X(y2-y_1)^2}{a^2r^3} - \frac{X}{r^3}\right]\mathrm{d}y2 \tag{18}$$

and the axial velocity increment is given by

$$\frac{U_{12B}(y_1)}{U} = \frac{-1}{4\pi^2}\int_{-b_2/2}^{b_2/2}C_{r2}C_{L\alpha\,3\mathrm{D}_2}\sin\alpha\frac{Z}{r^3}\sqrt{1-\left(\frac{2y_2}{b_2}\right)^2}\,\mathrm{d}y2 \tag{19}$$

For zero stagger, $X = 0$. Having determined the normal and axial velocity induced at any location of wing 1's bound vortex by wing 2's lifting elements, it is necessary to find the effect of these velocities on the lift.

Effect of the Induced Normal Wash on the Attached Flow Lift

The effect of the downwash on lift will be estimated using an equivalent two-dimensional lift-curve slope for the wing. From lifting line theory, the effect of the induced downwash can be interpreted to cause rotation of the local freestream such that the wing operates at an effective reduced angle of attack

$$C_L = C_{L\alpha\,3D}\alpha = C_{L\alpha\,2D}(\alpha - \alpha_i) \tag{20}$$

For the assumed elliptic loading, $\alpha_i = C_L/\pi AR$. Manipulation yields

$$C_{L\alpha\,2D} = \left[\frac{C_{L\alpha\,3D}}{1 - C_{L\alpha\,3D}/\pi AR}\right] \tag{21}$$

With this expression, the effect of the normal wash can be evaluated. For a delta wing, $C_{L\alpha\,3D}$ is closely approximated by[17]

$$C_{L\alpha\,3D} = 4\tan^{0.8}\epsilon \tag{22}$$

The change in the attached flow lift of wing 1 due to wing 2 is then (letting point of interest y_1 vary across the span as $y1$)

$$C_{L_{12}} = \frac{1}{b_1}\int_{-b_1/2}^{b_1/2} C_{L\alpha\,2D_1}\alpha_{12}(y1)\,dy1 \tag{23}$$

The effect of the bound vortex induced axial velocity increment on the attached flow wing lift curve slope is given by

$$C_{L\alpha\,3D_1}^{\cdot} = \frac{4}{\pi b_1}\int_{-b_1/2}^{b_1/2} C_{L\alpha\,3D_1}\left(1 + \frac{U_{12B}(y1)}{U}\right)\sqrt{1 - \left(\frac{2y1}{b_1}\right)^2}\,dy1 \tag{24}$$

The total attached lift of wing 1 is then (using $\sin\alpha$ to improve accuracy at high angles of attack)

$$C_{L1\text{at}} = C_{L\alpha\,3D_1}^{\cdot}\sin\alpha + C_{L_{12}} \tag{25}$$

Effect of the Induced Normal Wash on the Vortex Lift

In Polhamus'[10] expression for the vortex lift, K_V is affected by the lift-curve slope of the wing and the wing's aerodynamic efficiency, $\partial C_D/\partial C_L^2$. For a wing with elliptic loading, $\partial C_D/\partial C_L^2 = 1/\pi AR$. Deviation from elliptic loading may be incorporated through the use of an efficiency factor δ, which represents the increase in vortex drag from the planar unswept minimum. Thus, we may write $\partial C_D/\partial C_L^2 = (1+\delta)/\pi AR$ for a wing with non-elliptic loading. It follows that it is necessary to determine the effect of the downwash of wing 2 on the drag of wing 1. This drag variation will then be recast in terms of an increment relative to the monoplane wing, that is, δ. This allows straightforward incorporation into Polhamus'[10] formulation.

The normal wash of wing 2 on wing 1 effectively rotates the local freestream in the vicinity of wing 1, so tilting the resultant force causing an extraneous thrust or drag depending on the arrangement of the biplane cellule.

Using a far-field expression for the vortex drag of a wing gives the drag of wing 1 due to wing 2 (letting the point of interest y_1 vary as $y1$):

$$C_{D_{12}} = \frac{2}{S_1}\int_{-b_1/2}^{b_1/2}\frac{\alpha_{12}(y1)\Gamma_1(y1)}{U}\,dy1 \tag{26}$$

Substituting for Γ_1 and using $S_1 = C_{r1}\tan\epsilon_1$ yields

$$C_{D_{12}} = \int_{-b_1/2}^{b_1/2}\frac{-\alpha_{12}(y1)C_{L\alpha\,3D_1}2\sin\alpha}{\pi C_{r1}\tan\epsilon_1}\sqrt{1 - \left(\frac{2y1}{b_1}\right)^2}\,dy1 \tag{27}$$

where the negative sign is required due to the sign convention adopted; downwash results in positive drag. The monoplane vortex drag for wing 1 may be written as

$$C_{D_{1\text{mono}}} = \frac{\left(C_{L\alpha\,3D_1}\sin\alpha\right)^2}{\pi AR_1} \tag{28}$$

The efficiency factor to account for the influence of wing 2 on wing 1 is

$$\delta_{12} = C_{D12}\big/C_{D_{1\text{mono}}} \tag{29}$$

which, in the present analysis, is independent of α; this is not a result given by numerical lifting line theory.[18]

The vortex lift constant for wing 1, including the effects of wing 2, may now be written as

$$K_{V_1} = \left[C_{L\alpha\,3D_1}^{\cdot} - \frac{C_{L\alpha\,3D_1}^{\cdot 2}}{\pi AR_1}(1+\delta_{12})\right]\frac{1}{\cos\Lambda_1} \tag{30}$$

Thus, the increase in drag caused by interference (imbedded in δ_{12}) can be interpreted as a reduction in the wing's leading-edge suction and consequently vortex lift. To be consistent with Polhamus'[10] formulation, the effect of the net attached lift of wing 1 should be recast as an effective three-dimensional lift-curve slope given by

$$K_{P_1} = C_{L1\text{at}}\big/\sin\alpha \tag{31}$$

The final expression for the lift of wing 1 is

$$C_{L_1} = K_{P_1}\cos^2\alpha\sin\alpha + K_{V_1}\sin^2\alpha\cos\alpha \tag{32}$$

The coefficients in the preceding formulation were nondimensionalized by their respective areas (instead of the total cellule wing area, $S_1 + S_2$). For a biplane, calculation of C_{L1} and C_{L2} to give the total lift ($C_{L1} + C_{L2}$) would result in a lift coefficient value based on the area of each respective wing only (effectively one wing only for equal area wings). This form of presentation is useful in comparing the actual load carried by each wing to that of a monoplane and to ascertain relative and representative loading when the two biplane wings have dissimilar areas. If the lift coefficients based on the combined areas of both wings is desired, then the following formulas are used. This type of presentation is useful for evaluating the loading efficiency of the biplane as a whole and in determining overall interference effects:

$$C_L = \frac{S_1C_{L_1} + S_2C_{L_2}}{S_1 + S_2} \tag{33}$$

Similarly,

$$K_V = \frac{S_1K_{V_1} + S_2K_{V_2}}{S_1 + S_2} \tag{34}$$

$$K_P = \frac{S_1K_{P_1} + S_2K_{P_2}}{S_1 + S_2} \tag{35}$$

The preceding expressions were developed to determine the effect of wing 2 on wing 1. For computations, the effect of wing 1 on wing 2 is easily determined using the same expressions by reversing the signs of Z (gap) and X (stagger). If the wings are not of equal size, then the appropriate geometric values must also be changed. The wing to be evaluated is placed at the coordinate systems origin, and the other wing is positioned in accord with the desired gap and stagger. X and Z then indicate the location of the influencing wing, with consideration given to the axis convention. Computations consist of solving for the induced normal and axial wash [Eqs. (18) and (19)] and then integrating the velocity fields across the span using Eqs. (23) and (24) for the potential lift and lift-curve slope and using Eq. (27) for the vortex lift for wing 1, then repeating for wing 2. The total lift for each wing is determined using Eq. (32). The results are then combined using Eqs. (33–35). This can readily be accomplished using any commercial symbolic mathematics package. For a particular geometric configuration, only one computation per wing need be performed to find K_P and K_V (unless $Z/C_r < 0.25$ and the wing is at high α, then $K_V = f(\alpha)$, as will be discussed later), allowing prediction of the lift coefficient at any angle of attack within the range of the method's applicability.

As mentioned earlier, in the present method it is not necessary to know the exact location of the lifting lines relative to the wing chord. However, a complication arises in the definition of the gap between the wings. For a conventional unswept, untapered biplane system,

definition of the wing gap (usually Z/C_r) is unambiguous, and this property is constant along the span. For a delta wing, where physical properties scale with the local wing span, for example, circulation, a conventional definition of gap becomes dubious because the local semispan is variable. Consequently, it is more appropriate to use an averaged gap for a delta wing, which takes into account the slenderness of the wing. A natural formulation is

$$Z' = Z(b/C_r) = 2Z\tan\epsilon \tag{36}$$

Equation (31) should be used to define the gap in Eq. (4d). For unequal size wings, the use of the dimensions of the smaller wing is suitable.

It would be expected that the limitations of Polhamus'[10] suction analogy should extend to the present formulation. Accordingly, the present method should be limited to wings with $AR < 2$ and vortex breakdown free flow. For extremely slender deltas ($AR < 0.5$), merging of the leading-edge shear layers such that the flow no longer reattaches on the upper wing surface also limits applicability.

Comparison with Experiment and Theoretical Trends

In this section, comparisons will be presented of the prediction method with the experimental data as well as theoretically determined biplane parameter dependencies. Unless mentioned otherwise, the data have been presented using Eqs. (33–35), such that the coefficients are based on the total wing area. Consequently, the displayed data indicate directly the attenuation in wing loading compared to a monoplane (where these data are included) resulting from interference (not the actual lift that would be developed compared to the monoplane). Figure 6 presents the theoretical effect on $K_{Pu,1}$ and $K_{Vu,1}$ of the axial velocity increment induced by the wing's bound vortices, for zero stagger. The potential constant for the upper wing is increased and that for the lower wing is decreased, as follows from the directions of the velocity increments experienced at the wing's center lines. For equal strength vortex systems, the total K_P for the biplane wings is identical to that ignoring the axial

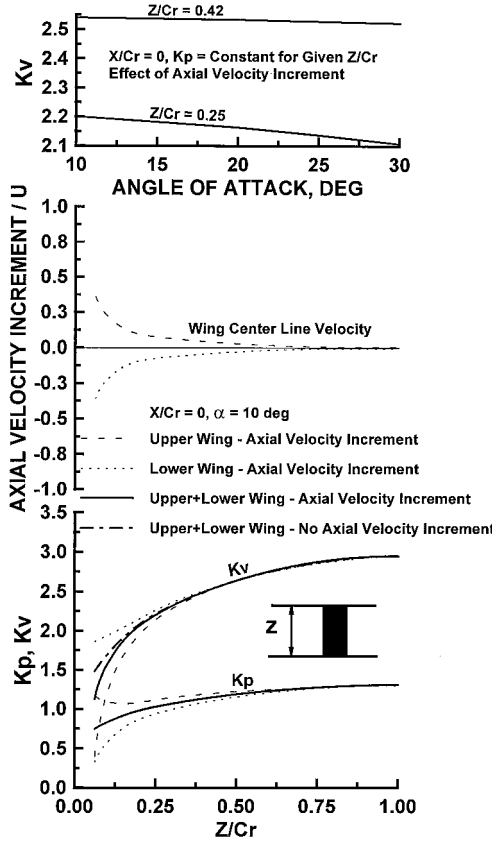

Fig. 6 Effect of the induced axial velocity increment/decrement on K_P and K_V of the individual wings and that of the cellule.

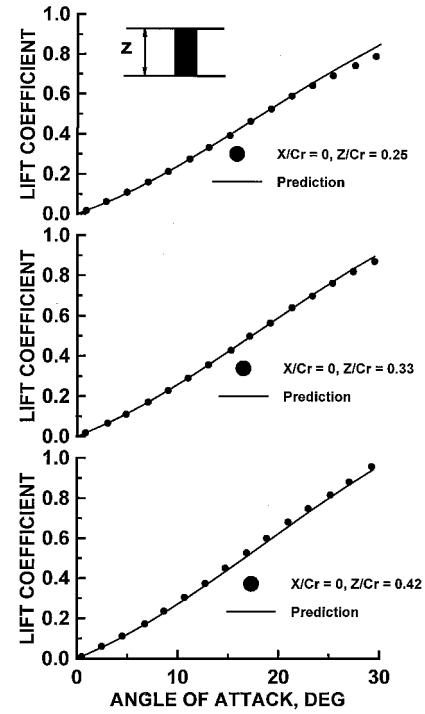

Fig. 7 Comparison of theory and experiment, effect of wing gap.

velocity increments; the increase and decrease in lift on the upper and lower wings, respectively, sum to zero.

Although not presented, the same result is found for stagger (this also follows from Munk's[6] stagger theorem as the lift in the present analysis is determined from the induced downwash). K_V, on the other hand, is affected by the induced axial velocities [due to the parabolic nature of the drag (second term on the right-hand side) in the leading-edge suction equation, Eq. (30)]. Consequently, the K_V increment/decrement for the upper and lower wings does not sum to zero. The effect is opposite to that expected, for example, a velocity increment on the upper wing decreases the vortex lift. This follows from Eq. (30) in that the wing lift-curve slope increases, but the wing slenderness (effected in AR and Λ) stays constant causing K_V to drop. Nonetheless, the axial velocity effect is seen to be small for $Z/C_r > 0.25$. Additionally, $Z/C_r < 0.25$ represents an extremely small and inefficient gap. The inclusion of the axial velocity increment results in K_V being dependent on α as shown in the top plot of Fig. 6. K_P, however, remains a constant, that is, $K_P \neq f(\alpha)$. The dependence of K_V on angle of attack is generally weak for $Z/C_r > 0.25$. As may be seen, increasing α reduces K_V and, thus, the vortex lift. The implication of $K_V(\alpha)$ is that for small wing gaps and high α, it is necessary to calculate K_V at regular intervals for best accuracy. Figure 7 presents a comparison of the experimental and predicted effect of the wing gap on C_L for zero stagger. Agreement between the theory and experiment is excellent, with a slight overprediction of C_L at high α for the smallest gap ($Z/C_r = 0.25$), which would be expected as vortex breakdown and wing–vortex proximity effects are not accounted for. The accurate prediction of the experimental data throughout the presented α range suggests that the present theory adequately predicts the biplane interference effects on both the attached flow (dominant at low α) and vortex lift (significant at high α). The ability of the method to predict lift for dissimilar sized wings is shown in Fig. 8. For this comparison, the cellule contains a small amount of positive stagger ($X/C_r = 0.05$ based on $C_r = 0.3$ m) and a gap of 0.42 (based on $C_r = 0.3$ m). Agreement is seen to be encouraging. The close accord demonstrated validates the simplifying assumptions applied in the theoretical formulation.

The explicit effect of gap on lift coefficient is examined in Fig. 9 for $\alpha = 10$, 20, and 30 deg. Data representing a monoplane wing are also included. The data show that the magnitude of the loss of lift compared to the monoplane increases with incidence. A comparison

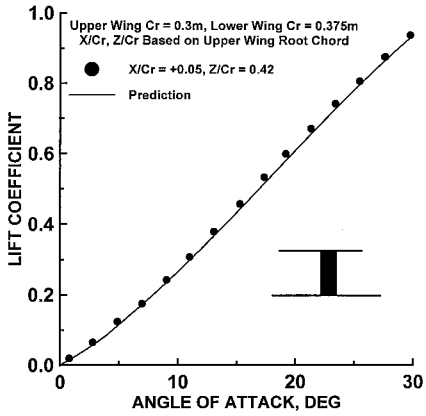

Fig. 8 Comparison of theory and experiment, dissimilar wing size.

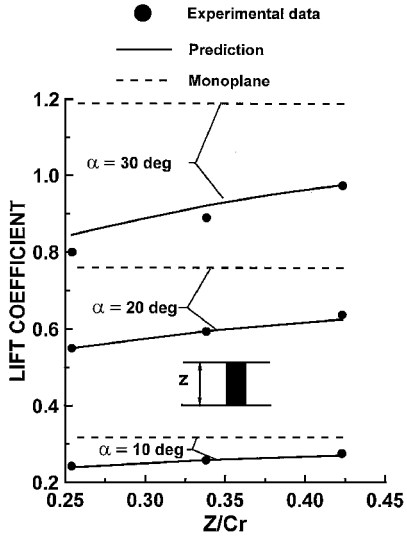

Fig. 9 Comparison of theory and experiment in effect of gap and α on lift.

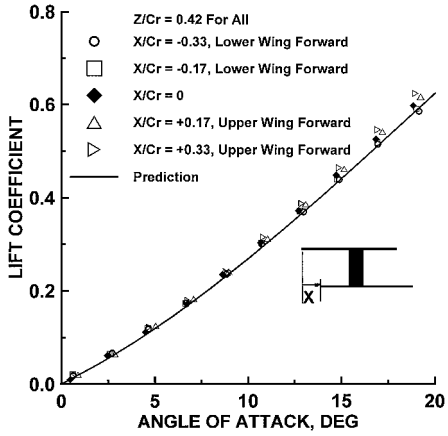

Fig. 10 Comparison of theory and experiment, effect of wing stagger.

of theory and experiment for the effects of stagger on lift coefficient are presented in Fig. 10. Theoretically, for this wing geometry, stagger has no effect on the total lift coefficient if the induced axial velocity effect is ignored and has a weak dependence (from K_V) if the axial effect is included for small Z/C_r and high α. At low angles of attack, $\alpha < 15$ deg, this consequence is supported by the experimental results. For $\alpha > 15$ deg, the experimental data display clear effects of stagger, largely due to wing–vortex interaction effects.

The effect of the wing gap on both K_P and K_V is shown in Fig. 11. The lower plot shows that K_P and K_V increase rapidly until $Z/C_r = 0.5$, which, as will be shown later, coincides with the behavior of the induced downwash on the wings. The upper plot in Fig. 11 presents K_P and K_V for the biplane reduced by the equivalent quantities for the monoplane wing. Note that for close wing proximity, that is, small Z/C_r, the vortex lift (reflected in K_V) is attenuated by the mutual wing interference to a greater extent than the potential lift (reflected in K_P). This characteristic diminishes with increasing Z/C_r and is not evident for $Z/C_r > 0.63$. The marked reduction in K_V for small gaps is largely a result of the axial velocity increment, as discussed earlier.

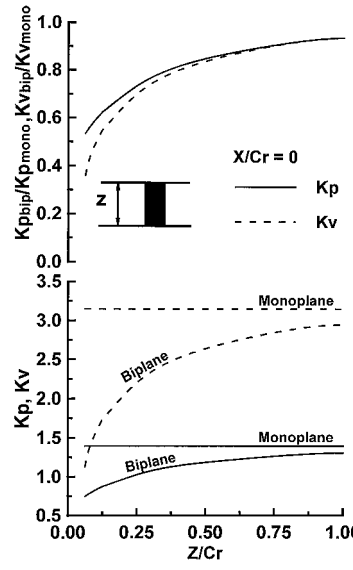

Fig. 11 Effect of wing gap on K_P and K_V.

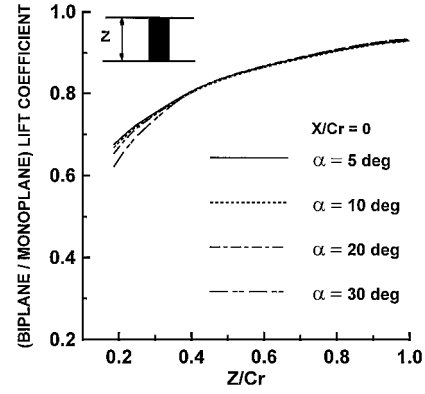

Fig. 12 Theoretical effect of wing gap and α on biplane to monoplane lift coefficient ratio.

The theoretical reduction in lift coefficient compared to a monoplane as a result of interference is illustrated in Fig. 12. The lift coefficient of the biplane as a function of monoplane lift coefficient for various gaps as well as that of α is examined. Interference effects are most pronounced for close proximity of the wings as the mutually induced downwash is large. The interference reduces for $Z/C_r > 0.5$ such that the lift of the biplane asymptotes toward that of the monoplane. For $Z/C_r = 1$, the biplane lift loading is approximately 92% of the monoplane. The lift ratio also demonstrates a dependence on α for close wing proximity. The attenuation of biplane lift for small Z/C_r and large incidence results in part from the dependence of K_V on α (see Fig. 6). The form of Fig. 12 appears logarithmic; this functional dependence is examined in Fig. 13 using a logarithmic scale for gap. As shown, the lift ratio displays a logarithmic dependence on gap.

Theoretical effects of stagger on the individual wing loading of the biplane cellule are presented in Fig. 14 ($Z/C_r = 0.42$). For equal strength vortex systems, the present theory predicts that stagger has no effect on the total lift of the biplane if the axial velocity effect [Eq. (19)] is neglected. It only affects the relative wing loading. As mentioned earlier, this characteristic is also seen experimentally (see Fig. 4), but is only evident for moderate wing angles of attack

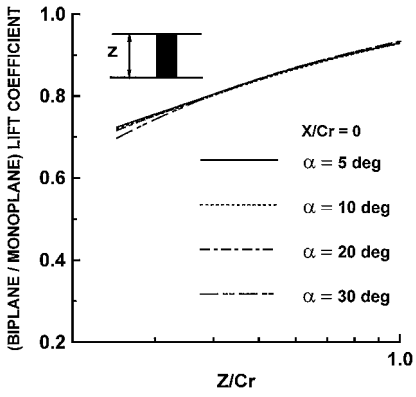

Fig. 13 Verification of logarithmic dependence of biplane to monoplane lift coefficient ratio on wing gap.

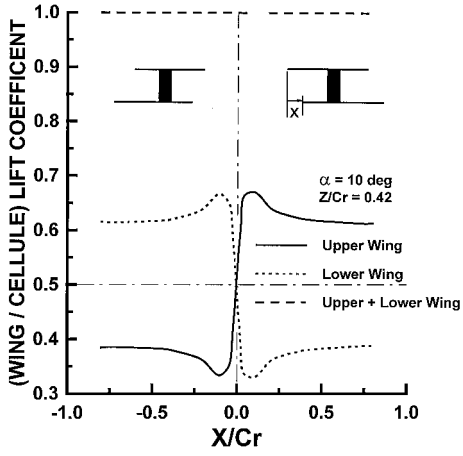

Fig. 14 Theoretical effect of wing stagger on individual wing loading, $Z/C_r = 0.42$.

(less than 15 deg), above which vortex–wing interaction effects may become pronounced. Including the effects of Eq. (19) causes C_L to be weakly dependent on stagger for small gaps and high α. Although K_P is unaffected by stagger, K_V does show a moderate dependence. For unequal strength vortex systems, for example, dissimilar wings, stagger effects the total lift (both K_P and K_V) whether Eq. (19) is included or neglected. For zero stagger ($X/C_r = 0$) the predicted loading on the upper biplane wing is slightly higher than the lower wing, due to the axial velocity increment/decrement (Fig. 14). If this effect were neglected, the loading would be equal. The relative invariance of the total lift is not too surprising if one considers two staggered lifting elements of equal strength. The effect of their bound vortex induced normal wash on the net lift is zero (as will be detailed later). For an unstaggered system the downwash experienced by the two wings is equal.

Upon staggering, the upwind wing is affected to a lesser degree by the other wing's trailing vortex system, whereas the induced downwash on the downwind wing increases proportionally. As $X/C_r \to \infty$, the upwind wing experiences no interference (and lift decrement), whereas the downwind wing is exposed to an infinite vortex system and, thus, experiences twice the downwash (and lift decrement) of the two wings with no stagger. Consequently, total lift is invariant. Mock[4] conducted an experimental study on an unswept high aspect ratio biplane configuration to determine the configuration's effect on the distribution of loading between the wings. His data show that for zero stagger and decalage, a weak interference effect is present such that the lower wing experiences a slightly larger loss of lift than the upper wing, a trend predicted in Fig. 14. This effect follows from the disparate axial velocities induced by the two wings' bound vortices; an increment on the upper surface and a decrement on the lower surface. Figure 14 shows that positive stagger increases loading on the upper wing and decreases it on the lower wing (vice versa for negative stagger); this follows from the bound vortex induced upwash of the lower wing on the upper wing for positive stagger. The influence of the bound vortex induced axial velocity increment/decrement for this configuration is weak and is reflected in slightly higher loading on the upper wing for positive stagger than on the lower wing for negative stagger. Initial displacement of the wings is seen to dramatically shift their relative load distribution, with this effect peaking around $X/C_r = 0.1$. This results from the strong initial influence of the wings' bound vortices. The behavior could not be validated by existing experimental data because the stagger increments used in the studies were too coarse.[2,4] Increasing the stagger beyond $X/C_r = 0.2$ significantly redistributes the load distribution between the wings. Expanding the wings' stagger further ($X/C_r > 0.4$) sees stabilization of the relative wing loading as the effect of both of the wing bound vortices diminishes. In addition, the interference from the trailing vortex induced downwash on the upper wing becomes negligible and that on the lower wing tends to a constant finite value. At this point, for positive stagger, the biplane interference effects manifest mainly on the lower wing and are dominated by the upper wing's trailing vortex system.

The effects of positive stagger on the induced angles of attack (W/U) are shown in Fig. 15 for $\alpha = 20$ deg. The data presented represent that induced on the designated wing, that is, the curves marked lower wing indicate the normal wash experienced by the lower wing due to the upper wing's vortex system. The normal wash angle has a linear dependence on $\sin\alpha$, but is presented dimensionally to convey the magnitude of the induced angles of attack. The nature of the data in Fig. 14 is clearly explained by the trends in Fig. 15. For moderate positive stagger ($X/C_r = 0.2$), the lower wing experiences significant downwash induced by the upper wing's bound and trailing vortices, causing a significant reduction in lift (Figs. 14 and 15). The upper wing experiences an upwash from the lower wing's bound vortex and a relatively small downwash from the lower wing's trailing vortex system. As a result, the wing experiences a net upwash and, thus, increased lift. The behavior of the induced upwash the upper wing experiences is responsible for the local loading peak shown in Fig. 14. For the lower wing, greater stagger has a weak effect on the downwash it experiences from the upper wing's trailing

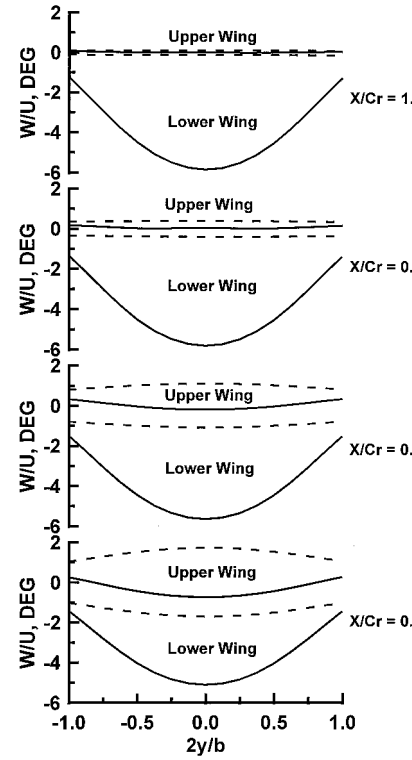

Fig. 15 Effects of wing stagger on the bound and trailing vortex contributions to the induced angles of attack, α = 20 deg: positive stagger, $Z/C_r = 0.42$, α = 20 deg; ——, trailing vortex contribution; - - - -, bound vortex contribution.

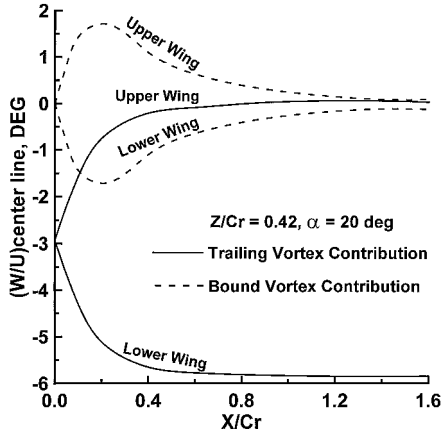

Fig. 16 Effects of wing stagger on the bound and trailing vortex contributions to the wing centerline induced angles of attack, $\alpha = 20$ deg.

vortex. Conversely, the bound vortex induced downwash diminishes progressively as shown in Fig. 15, causing the reduction of the lift decrement on the lower wing (see Fig. 14). For large stagger, the induced velocities experienced by the upper wing tend to zero due to increasing displacement from the lower wing's vortex system, both bound and trailing. The effects of negative stagger, under the simplifying assumptions of the present analysis, are identical but reversed. In Fig. 15 the result of negative stagger can be deduced by switching the labels for the upper and lower wing. Consequently a figure showing this is not included. An analogous argument to that presented explains the data in Fig. 14 for negative stagger.

It is instructive to gauge the chordwise variation of the induced normal wash at the wing center line as a function of X/C_r for the conditions presented in Fig. 15. As in Fig. 14, the wing designations indicate the normal wash induced on the named curve (by the other wing). This information is exhibited in Fig. 16 for positive stagger. The influence of the wing's bound vortex system is seen to increase rapidly with initial wing displacement, which, as shown in Fig. 14, has a profound effect on the relative wing loading. As seen, the upper wing experiences significant bound vortex induced upwash for positive stagger less than $0.8\ X/C_r$. The interference of the lower wing (on the upper wing) is essentially negligible for $X/C_r > 1.6$. For the lower wing, the downwash from the upper wing's trailing vortex system increases significantly initially and then asymptotes toward a constant value for $X/C_r > 1.2$. Conversely, the bound vortex interference (from the upper wing) on the lower wing increases rapidly until $X/C_r = 0.1$ and then diminishes swiftly for $X/C_r < 0.8$, tending to zero for larger stagger. Notice that the normal wash induced by the bound vortices of the two lifting elements is equal and opposite (see Figs. 15 and 16). This indicates that for wings with equal strength vortex systems the interference of the bound vortices has no effect on the total lift of the cellule, that is, the lift increment and respective decrement cancel out. Similarly, Munk[6] found that the total drag of a multiplane system can be determined ignoring any bound vortex contributions. The downwash on the lower wing is seen to have almost reached its final value (that is, for $X/C_r = \infty$) for $X/C_r > 1.2$, in that the downwash is approximately twice (indicating an effective infinite vortex system) that for no stagger.

The effects of the wing gap on downwash for $X/C_r = 0$ are shown in Fig. 17. For this case, the induced downwash is due only to the wings' trailing vortex systems and is equal for each wing. Data are also included for the variation of the downwash at the wing centerline with gap. For small gap ($Z/C_r = 0.1$) the induced downwash is relatively uniform along the center of the wing (this follows from the assumed elliptic loading: as Z/C_r tends to zero the induced downwash would become constant along the span). As the gap between the wings increases, the downwash reduces, becoming parabolic in form and ultimately tending to zero as Z/C_r tends to infinity. The nature of the downwash explains the trends seen in Fig. 12; for $Z/C_r > 0.5$ the induced downwash is reduced considerably. The

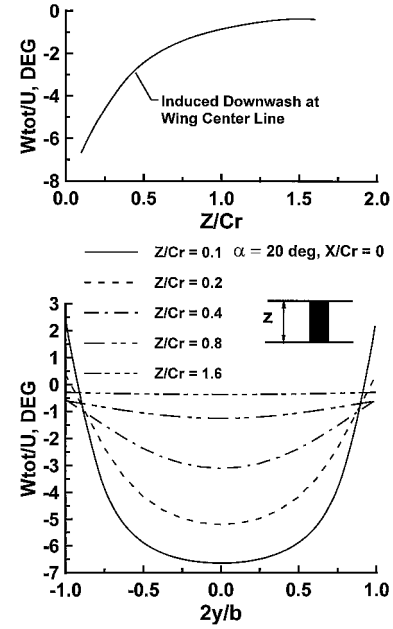

Fig. 17 Effect of wing gap on the trailing vortex induced centerline and spanwise downwash distribution.

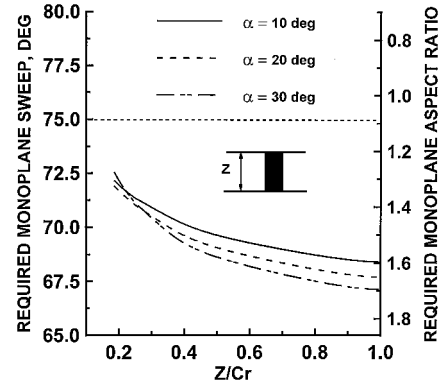

Fig. 18 Theoretically required monoplane delta wing AR and sweep to match lift of various biplane configurations.

general nature of this behavior is more clearly observed by variation of the wing centerline downwash; the resemblance between this plot and Fig. 12 is obvious.

The information presented prior was reduced by the total area of the biplane cellule. However, for a configuration with constrained projected dimensions, that is, a micro aerial vehicle, this form of data presentation may be misleading. It is more appropriate to present the data for a given lift ($C_L Sq$). It is instructive to determine the sweep of a delta wing that would be required to generate the same lift as the present biplane configurations. An expression that allows computation of the required sweep is readily determined using Eqs. (22) and (32) and is given by

$$C_{L\,\mathrm{bip}}(S_1 + S_2) = \left[4\tan^{0.8}\epsilon_{\mathrm{mono}} \sin\alpha \cos^2\alpha + \left(4\tan^{0.8}\epsilon_{\mathrm{mono}} - \frac{\left(4\tan^{0.8}\epsilon_{\mathrm{mono}}\right)^2}{4\pi \tan\epsilon_{\mathrm{mono}}} \right) \frac{\cos\alpha \sin^2\alpha}{\sin\epsilon_{\mathrm{mono}}} \right] C_r^2 \tan\epsilon_{\mathrm{mono}} \tag{37}$$

In evaluation, the computed lift coefficient (at a given α) and wing area for the biplane configuration is substituted into the left-hand side of Eq. (37). The expression is then solved for ϵ_{mono}. A typical result (assuming a constrained root chord, $C_r = 0.3$ m, and no stagger) is presented in Fig. 18. For any Z/C_r greater than approximately

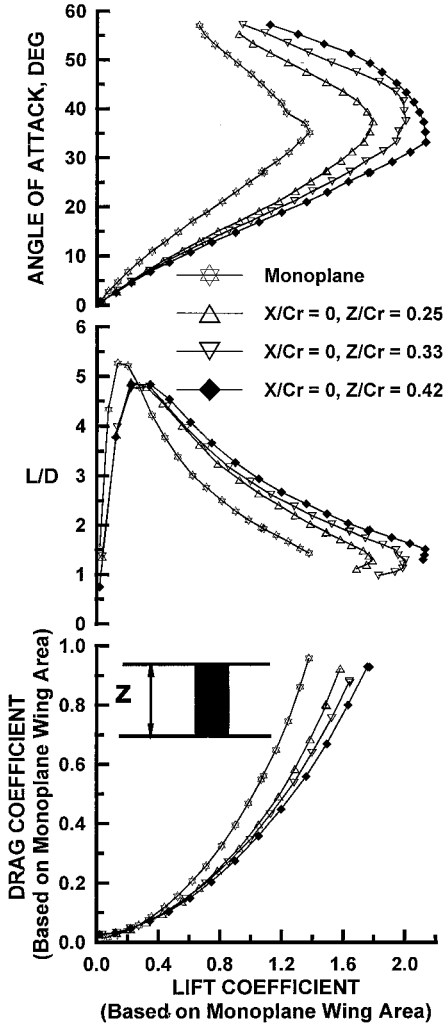

Fig. 19 Effect of wing gap on measured coefficients; presented data are equivalent to dimensional lift and drag.

0.1, a monoplane that matches the lift of the biplane requires a larger span and, thus, lesser sweep. This is pronounced for initial increases in the wing gap, and for $Z/C_r = 1$ a monoplane of approximately 68-deg sweep would be required. This wing represents a 51% increase in span and aspect ratio over the biplane. The higher aspect ratio of the monoplane also results in degraded high α performance following from the earlier onset of vortex breakdown. It may, thus, be inferred that for a constrained projected planform, a biplane is indeed a viable planform to generate the necessary lift to sustain a micro aerial vehicle. To improve the efficiency with which this lift is generated though, it is necessary to have wing gaps greater than $0.4C_r$.

Lift, drag, and the range parameter L/D for an unstaggered biplane and that of a monoplane representing one of the biplane wings is exhibited in Fig. 19. For a constrained planform vehicle, this comparison is representative. All of the presented data sets are reduced by the same area (that of the monoplane); thus, the information is equivalent to dimensional data. For lift coefficients less than 0.3, the increased wetted area of the biplane increases the skin friction, such that the monoplane has the lowest recorded drag and, as a result, the highest lift to drag ratio. For lift coefficients greater than 0.3, drag of the biplanes is markedly lower than the monoplane due to a significant increase in lift. The L/D ratio of all of the biplanes is notably improved over the monoplane, indicating a marked increase in potential range at higher lift coefficients. The effects of gap are only seen to manifest for lift coefficients greater than 0.4, with increasing gap augmenting lift.

Conclusions

A theoretical and experimental investigation was undertaken to determine the characteristics of delta wings in a biplane configuration. Wind-tunnel tests were undertaken using 75-deg delta wings, with variations in both wing gap and stagger. A theoretical method was developed that combined Prandtl's biplane theory[5] with Polhamus' leading-edge suction analogy.[10] From the experimental data the following conclusions are drawn: The separation between the wings has a significant effect on both the attached flow and vortex lift, both reducing with closer proximity of the wings. The biplane configuration shows far less sensitivity to stagger, with effects only manifesting for angles of attack greater than 15 deg. Positive stagger (upper wing forward) increased lift whereas negative stagger decreased lift relative to an unstaggered configuration. This result is in agreement with other studies. Similarly, positive stagger increased the maximum recorded lift coefficient, with negative stagger having the opposite effect. Positive stagger also improved poststall lift generation.

The theoretical method showed close accord with the experimental data and correctly predicted the effect of gap and stagger on lift. Theoretical analysis showed that for a dimensionally constrained planform, the delta wing biplane is an effective configuration for moderate to large wing gaps.

References

[1] Knight, M., and Noyes, R. W., "Wind Tunnel Pressure Distribution Tests on a Series of Biplane Wing Models Part II. Effects of Changes in Decalage, Dihedral, Sweepback and Overhang," NACA TN 325, Oct. 1929.

[2] Knight, M., and Noyes, R. W., "Wind Tunnel Pressure Distribution Tests on a Series of Biplane Wing Models Part I. Effects of Changes in Stagger and Gap," NACA TN 310, July 1929.

[3] Norton, F. H., "The Effects of Staggering a Biplane," NACA TN 70, Sept. 1921.

[4] Mock, R. M., "The Distribution of Loads Between the Wings of a Biplane having Decalage," NACA TN 269, Nov. 1927.

[5] Prandtl, L., and Tietjens, O.G., *Applied Hydro and Aeromechanics*, Dover, New York, 1934, pp. 211–222.

[6] Munk, M. M., "The Minimum Induced Drag of Aerofoils," NACA Rept. 121, 1921.

[7] Michelson, R., and Englar, R., "Micro Spy Planes, Inside the Worlds Smallest Aircraft," *Popular Science*, Jan. 1998, p. 53.

[8] Michelson, R. C., "Update of Flapping Wing Micro Air Vehicle Research," *Proceedings of the 13th Bristol International RPV/UAV Systems Conference*, Bristol, England, U.K., March–April, 1998.

[9] Traub, L. W., Moeller, B., and Redinitiotis, O. K., "Low-Reynolds-Number Effects on Delta-Wing Aerodynamics," *Journal of Aircraft*, Vol. 35, No. 4, 1998, pp. 653–656.

[10] Polhamus, E. C., "Prediction of Vortex-Lift Characteristics by a Leading-Edge Suction Analogy," *Journal of Aircraft*, Vol. 8, No. 4, 1971, pp. 193–199.

[11] Wentz, W. H., Jr., and Kohlman, D. L., "Vortex Breakdown on Slender Sharp-Edged Delta Wings," *Journal of Aircraft*, Vol. 8, No. 3, 1971, pp. 156–161.

[12] Kirby, D. A., "An Experimental Investigation of the Effect of Planform Shape on the Subsonic Longitudinal Stability Characteristics of Slender Wings," ARC, R&M 3568, 1969.

[13] Peckham, D. H., "Low Speed Wind Tunnel Tests on a Series of Uncambered Slender Pointed Wings with Sharp Edges," ARC, R&M 3186, 1961.

[14] Pope, A., and Rae, W. H., *Low-Speed Wind Tunnel Testing*, Wiley, New York, 1984, pp. 199–208, 362–424.

[15] Shindo, S., "Simplified Tunnel Correction Method," *Journal of Aircraft*, Vol. 32, No. 4, 1995, pp. 210–213.

[16] Jones, R. T., "Properties of Low Aspect Ratio Wings at Speeds Below and Above the Speed of Sound," NACA Rept. 835, 1946, pp. 59–63.

[17] Traub, L. W., "Prediction of Delta Wing Leading-Edge Vortex Circulation and Lift-Curve Slope," *Journal of Aircraft*, Vol. 34, No. 3, 1997, pp. 450–452.

[18] von Mises, R., *Theory of Flight*, Dover, New York, 1959, p. 253.